Clinically visible progression indicators in age-related macular degeneration are transdifferentiated retinal pigment epithelium

Dongfeng Cao PhD[1‡], Belinda Leong MD[2,4‡], Jeffrey D. Messinger DC [1], Deepayan Kar MS [1], Thomas Ach MD[5], Lawrence A. Yannuzzi MD [2,3], K. Bailey Freund MD[2,3,6,], Christine A. Curcio PhD[1]*

[1]Department of Ophthalmology and Visual Sciences, University of Alabama at Birmingham School of Medicine; Birmingham, AL, USA.

[2]Vitreous Retina Macula Consultants of New York; New York, NY, USA.

[3]LuEsther T. Mertz Retinal Research Center, Manhattan Eye, Ear and Throat Hospital; New York, NY, USA.

[4]Retina Associates; Sydney, NSW, Australia.

[5]Department of Ophthalmology, University Hospital Bonn; Bonn, Germany.

[6]Department of Ophthalmology, New York University, Grossman School of Medicine; New York, NY, USA.

***Corresponding author. Email: christinecurcio@uabmc.edu**

‡These authors contributed equally to this work.

Words: 9622 (main), **Figures:** 6; **Supplementary figures:**10; **Supplementary tables:** 7

One Sentence Summary

In age-related macular degeneration retinal pigment epithelial cells transdifferentiate and migrate into the retina where they are clinically visible progression risk indicators.

Abstract

Age-related macular degeneration (AMD) is a common sight-threatening disease of older adults and treatment options are needed. Abnormalities of retinal pigment epithelium (RPE), supporting cells to photoreceptors and capillaries, are a hallmark. Clinical optical coherence tomography (OCT) imaging reveals hyperreflective foci (HRF) that confer risk for end-stage disease and are attributed to ectopic out-of-layer RPE. Using longitudinal OCT imaging of AMD patients, we demonstrate that the trajectory of one HRF form, RPE plume, parallels the retinal Henle fiber layer. Histology shows fully pigmented cells approaching and contacting retinal capillaries with RPE organelles dispersing along Müller glia columns. We used immunohistochemistry and a system of morphologic phenotypes to assess RPE functional repertoire in AMD. RPE corresponding to HRF loses immunoreactivity for retinoid processing proteins RPE65 and CRALBP, and gains immunoreactivity for immune cell markers CD68 and CD163. Müller glia retain CRALBP immunoreactivity. Gain- and loss-of-function for RPE starts with individual in-layer cells and extends to all abnormal phenotypes. Down-regulated RPE retinoid handling may contribute to slowed rod vision while Müller glia sustain cone vision. Ectopic RPE corresponding to HRF are emblematic of widespread transdifferentiation, motivating treatments targeting AMD pathology earlier than the initiation of atrophy. Data can propel new biomarkers and therapeutic strategies for AMD.

Abbreviations: AMD, Age-related macular degeneration; BLamD, basal laminar deposit; BrM, Bruch's membrane; Ch, choroid; ChC, choriocapillaris; cRORA, complete RPE and outer retinal atrophy; d, drusen; ELM, external limiting

membrane; EZ, ellipsoid zone; fv scar, fibrovascular scar; GCL, Ganglion cell layer; HFL, Henle fiber layer; ILM, internal limiting membrane; IPL, inner plexiform layer; INL, inner nuclear layer; IS, inner segments of photoreceptors; iRORA, complete RPE and outer retinal atrophy; IZ, interdigitation zone; nvAMD, neovascular AMD; ONL, outer nuclear layer; OPL, outer plexiform layer; OS, outer segments of photoreceptors; R, retina; Sc, sclera; SRS, subretinal space; x, detachment.

INTRODUCTION

Age-related macular degeneration (AMD) causes vision loss in older persons worldwide (*1*). Neovascular complications are managed medically (*2*), whereas the underlying and prevalent atrophic ("dry") disease is not yet treatable. AMD affects vertically integrated cellular layers formed by light-sensing photoreceptors and support cells (retinal pigment epithelium (RPE), choriocapillaris, Müller glia). Characteristic extracellular deposits (drusen, subretinal drusenoid deposits) form between photoreceptors and their choroidal and retinal blood supplies (*3*). RPE cells supporting photoreceptors and vessels are central to, and impacted by, both atrophic and neovascular AMD.

AMD is increasingly understood via clinical imaging, particularly optical coherence tomography (OCT). This technology provides depth-resolved views of retinal and choroidal tissue layers (*4*) and is amenable to histologic validation (*5*). A progression sequence for drusen-initiated atrophy is age-related deterioration in choriocapillaris and Bruch's membrane (a vascular wall) preventing egress of wastes to the circulation, growth of drusen with death or migration of overlying RPE, and reactive gliosis (*5*). To the vision-initiating photoreceptors, AMD is a disease of the re-supply route for retinoids (vitamin A derivatives) translocated from the circulation across the affected tissue layers

74 (*6*). Rod-mediated (dim light) vision is affected first, because rods depend on these
75 layers (*7*). Cone-mediated (bright light) vision, also sustained by Müller glia and retinal
76 vessels (*8*), persists into later disease. In this overall model, the RPE is a readout of
77 pathology in the less visible Bruch's membrane and choriocapillaris. RPE fate in AMD
78 can be uniquely monitored in vivo, because each cell has >1400 organelles (*9*) capable
79 of generating OCT signal, and OCT is widely used in the management of neovascular
80 AMD.

81 Longitudinal studies and post-hoc analysis of clinical trial imaging datasets
82 revealed OCT biomarkers for progression from intermediate AMD to geographic atrophy.
83 Tissue damage in atrophy is severe and possibly irreversible (*10*). Identifying trial
84 outcome measures earlier than expansion of atrophy, currently the only measure
85 accepted by the U.S. Food and Drug Administration, is the goal of an international
86 consensus group (*5, 11-13*). Of OCT biomarkers, hyperreflective foci (HRF) within the
87 neurosensory retina confer the largest risk for progression (*14-17*). HRF correspond to
88 ectopic RPE that detach from the layer and migrate anteriorly. A histologic survey of
89 RPE phenotypes (*18-20*), confirmed in clinically characterized eyes (*18, 21*), identified
90 two phenotypes corresponding to HRF, "sloughed" (among the photoreceptors) and
91 "intraretinal" (within the neurosensory retina). In a hypothetical progression sequence
92 (fig. S1), morphologically distinct cells deploy along separate pathways of cell fate,
93 including death, migration, and transdifferentiation to other cell types, without intervening
94 dedifferentiation and proliferation (*22*). Due to migration and death-in-place of RPE, the
95 layer disintegrates, scattering fully pigmented and nucleated cells ("dissociated") across
96 atrophic areas. Some cells appear to dive below the intact layer and migrate outside the
97 atrophic area ("subducted") (*19*).

98 To investigate whether one HRF form called “RPE plume” exhibits the behavior of
99 cells crossing the retina in parallel with the Henle fiber layer (HFL) (fig. S2), we herein
100 provide a clinical OCT timeline for this feature in patients with AMD. Applying
101 immunohistochemistry of human donor eyes to test whether HRF are transdifferentiated,
102 we show loss of retinoid processing and gain of immunologic function in all abnormal
103 RPE phenotypes. To complete a HRF lifecycle, we show RPE-derived debris in relation
104 to the cross-retinal course of Müller glia. Because RPE transdifferentiation is
105 widespread, a strategy of visualizing and targeting pathology earlier in AMD progression
106 than atrophy is warranted.
107

108 **RESULTS**

109 **Clinical imaging**

110 Four morphologies of RPE plume were defined (Fig 1). Curvilinear plumes (Fig. 1A)
111 appear as hyperreflective features of constant width, above the RPE layer with or
112 without drusen, and pointing towards the outer plexiform layer. Relative to curvilinear,
113 comma plumes (Fig. 1B) are similarly reflective, with a wider base at the RPE layer and
114 tapering anteriorly. Like curvilinear, thread plumes (Fig. 1C), previously seen in inherited
115 retinopathies (*23*), are of uniform width but are thinner. A vitelliform plume (Fig. 1D) is
116 thick at its base, typically an acquired vitelliform lesion (autofluorescent and yellow
117 subretinal extracellular material) (*24*), with an anterior taper that widens over time.

118 To observe plume lifecycles and intraretinal trajectories, 44 patients with non-
119 neovascular AMD (61 eyes, 29 females, 79.4 years (standard deviation 7.7 years)) with
120 at least one HRF and mean follow-up duration of 4.67 years (standard deviation 0.09
121 years) were enrolled (table S1). In 29 eyes of 21 patients (15 female), 129 plumes were
122 followed for locations and characteristics including presence of complete and incomplete
123 RPE and outer retinal atrophy (cRORA, iRORA) (*5, 12*). Plumes obliquely crossing
124 horizontally oriented OCT B-scans appeared as small reflective dots that were
125 connected by inspecting consecutive scans (fig. S3). Over time individual plumes
126 evolved considerably (Fig. 2), converting from one morphology to another (Fig. 2A to 2E)
127 or to discrete HRF (i.e., unconnected to the RPE layer) (Fig. 2A and 2F), disappearing
128 with (Fig. 2A, 2C and 2D) or persisting after (Fig. 2A, 2C and 2E) druse collapse to
129 atrophy, or even predating druse appearance (Fig. 2E).

130 Curvilinear and thread plumes were the most common morphologies at baseline
131 and the longest lasting over follow up (fig. S4A). Plume number and dynamism (i.e.,

132 appearance, disappearance, and conversions) could be striking (fig. S4B). Of 129
133 plumes at baseline (table S2), 73 (56.5%) converted to another plume morphology or
134 discrete HRF during follow-up, with 38 disappearing and 35 remaining; 56 (43.4%)
135 plumes retained the original morphology.

136 Most plumes (101/129, 78.2%) were geometrically congruent with the local
137 trajectory of the normal HFL (table S3), especially temporal to the fovea, with more non-
138 congruent plumes superior nasal to the fovea. Of 129 plumes, 73/129 (56.5%) were
139 associated with cRORA. Near cRORA, plumes were seen traveling in directions
140 unrelated or opposite to the normal HFL (fig. S5). Accordingly, at the final visit (table S4),
141 43/129 (33.5%) plumes associated with cRORA were congruent with the local normal
142 HFL and 25/129 (19.3%) were incongruent, with 16/129 (12.4%) of incongruent plumes
143 located at the cRORA border. In contrast, all 6/129 (4.7%) plumes associated with
144 iRORA were congruent with the HFL. Finally, 50/129 (38.8%) of plumes were not
145 associated with either cRORA or iRORA.
146

147 **Laboratory study**

148 To molecularly characterize cells corresponding to HRF, in the context of overall RPE
149 perturbation in AMD, we first used *ex vivo* OCT imaging to find human donor eyes with
150 AMD (fig. S6) and then confirmed diagnosis with histology. HRF found in OCT B-scans
151 of the macula were matched with pigmented cells in the subretinal space and retina of
152 stained sections (fig. S6). Atrophic AMD eyes with RPE plume in OCT exhibited
153 pigmented cells in the outer nuclear layer (ONL) and HFL on histology (fig. S6, C1 to C2
154 and F1 to F2). Twenty eyes of white donors (mean age 89.2 ± 5.0 years; 16 AMD, 4

155 control), with mean time from death to preservation of 3.9 ± 0.7 hours (table S5), were
156 studied.

157 To elucidate the molecular repertoire of abnormal RPE, including “sloughed” and
158 “intraretinal” phenotypes corresponding to HRF, we provide immunohistochemical
159 evidence for both gain-of-function and loss-of-function using antibodies for retinoid- and
160 immune-related proteins detailed in table S6 and appropriate positive and negative
161 controls in human tissues shown in fig. S7. To contextualize staining, we checked the
162 immunolabeling of all phenotypes (*25*) (table S7) using bright field microscopy for direct
163 observation of cellular pigmentation and status of surrounding tissue.

164 We begin by demonstrating that cells of RPE origin label with antibodies against
165 two well-known immune cell markers, Cluster of Differentiation (CD)68 and CD163 (*26*).
166 CD68 is a transmembrane glycoprotein that is abundantly expressed by macrophages
167 and widely used as a myeloid-specific marker (*27*). CD68 is one member (LAMP-4) of a
168 5-protein family that together accounts for 50% of the protein in lysosome membranes
169 (*27*). In human chorioretinal tissue sections Fig. 3, positive controls for CD68
170 immunoreactivity are choroidal macrophages (Fig. 3D) and negative controls are healthy
171 RPE (Fig. 3A). Fully pigmented cells in the neurosensory retina are strongly CD68+ (Fig.
172 3F). Importantly, individual sloughed cells in the subretinal space (Fig. 3C and 3F) are
173 also positive, as are individual cells still within the layer (Fig. 3E). Dissociated RPE
174 scattered in the atrophic area are universally labeled (Fig 3H and 3N), as are cells under
175 the continuous layer (Fig. 3I), and within outer retinal tubulation (Fig. 3J and 3K), i.e.,
176 tubes of scrolled photoreceptors (*28*). Some bilaminar (Fig. 3D) and melanotic (Fig. 3M)
177 cells are CD68+.

178 CD163 is a high-affinity haptoglobin-hemoglobin scavenger found in bone marrow-
179 derived macrophages (*29*) and in retinal cells resembling microglia (*30-32*). The latter
180 are phagocytes of embryologic yolk sac origin that reside in inner retina when quiescent
181 and migrate into outer retina when photoreceptors are damaged (*30*). Fig. S8 shows that
182 anti-CD163 labels inner retina cells but not the normal RPE layer, as expected. It does
183 label abnormal RPE phenotypes in a pattern like that of CD68, with overall lighter
184 reaction product. These include fully pigmented CD163+ cells in the ONL (fig. S8, F and
185 N), HFL (fig. S8L), above (fig. S8, E and I) and below (fig. S8I) the continuous RPE layer
186 in the subretinal and sub-RPE-basal laminar spaces, respectively, and dissociated cells
187 in atrophic areas (fig. S8, H, J and K).

188 Next, we show that abnormal RPE cells cease to express detectable quantities of
189 retinoid processing proteins. We begin with RPE65, the isomerohydrolase of the classic
190 visual cycle. RPE65 catalyzes the conversion of retinyl esters to 11-cis-retinol, which is
191 subsequently oxidized to 11-cis-retinal, required for visual transduction by rod and cone
192 photoreceptors (*33*). Figure 4 shows that in AMD eyes, intraretinal RPE in ONL (Fig. 4F)
193 and individual sloughed cells overlying the continuous layer (Fig. 4, C and L) lack
194 RPE65-immunoreactivity. Cells in areas of photoreceptor degeneration and depletion
195 are also RPE65-, including dissociated (Fig. 4N), subducted (Fig. 4I) and entubulated
196 (Fig. 4J) cells. Importantly, some individual cells in the continuous layer are RPE65-
197 (Fig.4, F and H). Interestingly some bilaminar cells within fibrotic scars of neovascular
198 AMD remain RPE65+ (Fig. 4M).

199 Cellular retinal binding protein (CRALBP), in addition to participating in the RPE-
200 based visual cycle, is also expressed by Müller glia in a second visual cycle supplying
201 only cones (*8, 34*). CRALBP is a 36-kDa water-soluble protein with 2 conformational

202 states facilitating intracellular transport of hydrophobic 11-cis retinoids (*35*). Fig. 5 shows
203 that healthy RPE has a strong CRALBP signal (Fig. 5A) as do Müller glia (Fig. 5E). In
204 AMD, ectopic RPE in the ONL, recognizable by pigmentation and granule load, are
205 CRALBP- (Fig. 5F and L). Individual sloughed cells (Fig. 5, H and L) and cells in the
206 continuous layer (Fig. 5E) are also negative as are pigmented cells in atrophic areas
207 (dissociated, Fig. 5, C, K and N; subducted, Fig. 5I). Shed granule aggregates (*18, 36*)
208 are CRALBP- under a CRALBP+ layer (Fig. 5B). Regardless of the degree of
209 photoreceptor loss (Fig. 5, C, J, K and N), Müller glia remain strongly CRALBP+ in their
210 cross-retinal course. This includes the external limiting membrane, i.e., junctional
211 complexes between glia and photoreceptors (*37*). In the HFL stained Müller glia are
212 parallel and straight in areas of lesser disease involvement (ordered (*10*), Fig. 5L). At the
213 border of atrophy (descent of the external limiting membrane (*38*), Fig. 5, C, K and N)
214 and outer retinal tubulation (Fig. 5J), CRALBP+ fibers curve down towards Bruch's
215 membrane and then head laterally, parallel to it. In some locations immunolabeled fibers
216 zig-zag in parallel, presenting cross-sections of dots and lines (disordered (*10*), Fig. 5, F
217 and N). CRALBP signal also appears in fibrotic scars resulting from neovascular AMD
218 **(**Fig. 5, D, G and M).
219 The number of stained cells in each RPE phenotype was assessed a semi-
220 quantitatively (0, not stained; 1, some cells of a phenotype stained; 2, all cells stained).
221 These scores were summed and expressed as a percent of the highest possible score,
222 as if all phenotypes had been stained completely by each antibody. Figure S9A shows
223 that the RPE phenotypes seen in these 16 AMD eyes were found in all the immuno-
224 stained sections. Figure S9B graphically summarizes the marker studies. Age-normal
225 uniform and non-uniform RPE is positive for retinoid markers and negative for immune

226 markers. Abnormal RPE phenotypes have overall less retinoid immunoreactivity
227 (although some stained cells were found) and universally more immune marker
228 immunoreactivity. Thus, cells corresponding to HRF in OCT are part of an overall pattern
229 of transdifferentiation resulting in gain-of-function and loss-of-function of RPE.
230 Our clinical study indicated that RPE plume like other OCT features in AMD has a
231 lifecycle. We previously showed in type 3 (intraretinal) neovascularization that RPE cells
232 contact the deep capillary plexus, suggesting ischemia due to choroidal insufficiency as
233 a precipitating event to anterior migration (*21*). We thus examined the trajectory of plume
234 cells at higher detail (Fig. 6). In Fig. 6, A to C, RPE cells in a plume are seen crossing
235 the HFL to approach and encircle capillaries of the deep plexus. Cells are nucleated and
236 contain numerous RPE-characteristic spindle-shaped melanosomes and
237 melanolipofuscin granules, in processes that extend along the capillaries (Fig. 6D).
238 We previously showed RPE organelles in the HFL of photoreceptor-depleted
239 atrophic areas (*10*), suggesting that Müller glia ingested and cleared debris from
240 degenerating RPE. Here we show region-specific distribution of RPE organelles,
241 consistent with the local trajectory of Müller glia. In the macula, Müller glia are Z-shaped
242 (*39*), because obliquely oriented fibers in the HFL verticalize at the border of OPL and
243 inner nuclear layer (fig. S2). In plumes near the fovea (Fig. 6, E and F; and fig. 8N), fully
244 pigmented RPE cells cross the obliquely oriented HFL, with individual and grouped
245 organelles in the lead. The path turns vertically to enter and cross the INL and IPL,
246 taking a Z-shaped course. In contrast, in the peripheral retina, where Müller glia are
247 vertical, fig. S10 shows melanosomes following a vertical track away from the RPE
248 above a druse.
249

250 **DISCUSSION**

251 Widespread clinical use of OCT has enabled visualization of smaller and thus earlier
252 stages of RPE pathology than the pigmentary changes known from color fundus
253 photography to confer progression risk (*40*). HRF are one of four OCT indicators in a
254 composite risk score for AMD progression risk (with soft and calcified drusen, plus
255 subretinal drusenoid deposit) (*41*). HRF confer the largest risk of these four indicators
256 (odds ratio, 5.21 (3.29-8.26) at 24 months))(*16*) and are the last to receive histologic
257 investigation. For RPE plume, an HRF with specific morphologies and behavior, we
258 establish a lifecycle including both cRORA and resolution without cRORA. We further
259 show that cells corresponding to HRF (sloughed and intraretinal) are two of many
260 abnormal RPE phenotypes undergoing molecular transdifferentiation in AMD.

261 Our parallel findings of CD68 and CD163 immunoreactivity in all abnormal RPE
262 phenotypes adds important new information to a decades-old debate (*42*) about whether
263 RPE, a phagocyte itself, shares or assumes properties of other phagocytes. This
264 investigation like our previous studies used high resolution comprehensive microscopy
265 to link cells with characteristic RPE organelles (*18, 19*) to a time course of activity visible
266 through longitudinal clinical imaging. Our cellular phenotyping system (*18*) built on prior
267 literature and is used by others (*43, 44*). We posited that these phenotypes represented
268 discrete steps towards death, migration, or transdifferentiation of individual cells that
269 could be followed over time in OCT due to high RPE reflectivity. In prior electron
270 microscopic analysis of pigmented cells corresponding to HRF (*45*), we did not observe
271 phagolysosomes, i.e., cytoplasmic vacuoles formed by phagosomes with ingested
272 material fusing with lysosomes, as expected from phagocyte activity. In a separate study
273 of HRF over a large drusenoid pigment detachment (*20*), all HRF could be attributed to

274 fully pigmented and nucleated intraretinal cells. In clinical cases of that prior study (*20*),
275 HRF appeared in the retina vertically above and several months after disturbances of the
276 RPE layer. Our current data further show that individual in-layer cells and all abnormal
277 phenotypes exhibit CD68 and CD163 immunoreactivity. We cannot entirely exclude the
278 possibility that phagocytes ingest and retain characteristic RPE organelles, seamlessly
279 intercalate into the layer, and either become abnormal phenotypes or induce them.
280 However, extensive transdifferentiation in response to common perturbations is also a
281 parsimonious explanation.

282 We emphasize that detection of CD68, a lysosomal protein of unknown function
283 reliably found in macrophages of myeloid origin (*27*), at one time point does not indicate
284 that immunoreactive pigmented cells have assumed macrophage behavior. Our data do
285 not imply that macrophages of hematopoietic origin previously documented in choroid
286 and sub-RPE-BL space (*46, 47*) actually started as RPE. Our data do not bear on the
287 identity of CD68+ cells seen by others, e.g., high-passage cultured RPE (*48*) and
288 surgically excised neovascular membranes (*49, 50*). Following experimental laser-injury
289 and rapid preservation, individual detached cells atop an intact RPE layer are CD68+
290 (*51*) resembling Fig. 3C and fig. S8C. Recent authors interpreted CD68+ cells in
291 aqueous after RPE tear (*52*) and in proliferative vitreoretinopathy (*53*) as RPE. A layer of
292 CD68+ cells in the outer junctional zone of atrophy in AMD was demonstrated by
293 immunofluorescence and laser confocal microscopy (*43*). This technique does not
294 directly reveal melanin, and the authors did not comment on cellular identity (*43*).

295 Our data further illuminate subducted cells on the inner collagenous layer of
296 Bruch's membrane, containing RPE organelles and originally called "spent RPE" (*54*). In
297 prior studies of single continuous high-resolution histologic sections of eyes with

298 cRORA, we saw plausible transitional morphologies between fully pigmented RPE
299 outside atrophic areas and flattened cells with fewer organelles in the sub-RPE-BL
300 space (*19*). We thus hypothesized that dissociated RPE in the central atrophic area,
301 loosed from constraining junctional complexes, dove under the layer and moved laterally
302 (*55*) into the outer junctional zone (*19*). Herein we show CD68+ and CD163+ cells and
303 highly pigmented RPE65- and CRALBP- cells in the same sub-RPE-BL tissue
304 compartment of the same eyes. Definitive multi-label immunohistochemistry is needed to
305 confirm whether these are all RPE-derived subducted cells. Further, the narrow sub-
306 RPE-BL space is known to contain macrophages of myeloid origin, multinucleate giant
307 cells, and fibroblasts (*56*). It is possible that co-localized CCR2 and CD18
308 immunoreactivity in these locations, attributed to macrophages (*57*), may represent
309 subducted and dissociated RPE, respectively. A plausible progression sequence based
310 on cellular phenotype and longitudinal imaging (fig. S1) offers a perspective on lineage
311 tracing independent of molecular marker snapshots (*57*).
312 A spreading outward of subducted cells may contribute to atrophy expansion
313 beyond degeneration of RPE and photoreceptors and gliosis. Macrophages that co-
314 express CD68 and CCR7 can be assigned to a ‘‘proinflammatory’’ M1 subset, whereas
315 CD68+ CD163+ macrophages most likely belong to an ‘‘anti-inflammatory’’ M2 subset
316 (*58*). Longitudinal studies with next-generation high-resolution OCT (*59, 60*) may allow
317 tracking of subducted cells to see if they promote or retard atrophy expansion. Such
318 information will be highly valuable, because expansion is the only regulatorily-approved
319 anatomic endpoint for clinical trials.
320 Our expectation of plume congruence with HFL trajectory was largely met and of
321 note was non-congruence near cRORA (table S4). This is likely due to subsidence

322 (sinking) of the OPL, HFL, and ONL, a committed step toward cRORA onset (*61*).
323 Subsidence is visible where photoreceptors focally shorten and are scrolled by Müller
324 glia (*10, 62*). Our data on plume trajectories and CRALBP immunohistochemistry thus
325 add to prodigious activities of Müller glia in AMD. These include descent and curving of
326 the ELM (border of atrophy), reactive gliosis, adherent glial seal in areas of
327 photoreceptor depletion, and invasion of individual drusen (*28, 38, 63, 64*). Parallelism of
328 HFL fibers contributes to high light transmittance in healthy retina; HFL reflectivity
329 increases focally when disturbed (*65, 66*). CRALBP immunohistochemistry confirmed
330 HFL fiber geometry as well as retinoid capacity of Müller glia, still supported by retinal
331 circulation late in disease. Single and grouped RPE organelles paralleling Müller glia
332 (*10, 67*) are presumably carried intracellularly. In contrast RPE cell bodies traveling
333 between HFL fibers (Fig. 5L and Fig. 6) following a trail of organelle detritus. Active glial
334 disassembly and removal of fragments is suspected.
335 Because almost 40% of plumes were not associated with atrophy at follow-up
336 (table S4), plumes should be considered indicators not predictors. Factors underlying
337 variable plume outcome in our study include inclusion of patients with established
338 disease, short observation period, and a “come and go” behavior consistent with cells
339 subject to constant pro-migratory stimuli being dismantled *en route*. Given our evidence
340 for widespread transdifferentiation, HRF including plumes may indicate risk by revealing
341 an overall level of disease activity not only in the RPE layer but also in less-visible
342 adjacent tissue layers (e.g., drusen-associated lipid peroxidation in the sub-RPE-BL
343 space, Bruch’s membrane cross-linking, loss of choriocapillary endothelium (*68-70*)).
344 These collectively impair bi-directional exchange between outer retina and the circulation
345 and introduce pro-inflammatory, pro-angiogenic compounds. A major role for ischemia

346 due to vascular insufficiency is underscored by evidence for RPE cells contacting retinal
347 capillaries (Fig. 6; (*20, 21*)). Our demonstration of fully pigmented plume cells aiming
348 towards and clustering around the deep capillary plexus (Fig. 6) further supports the idea
349 that the cells are RPE in transit and not phagocytes. They apparently move as a
350 coordinated group rather than as single cells that go to vessels and proliferate. Similar
351 conclusions about an inductive role of vascular insufficiency have been reached for
352 neovascularization of choroidal origin (*71*). Finally, a visual task limited by retinoid
353 resupply from the circulation (*7*), rod-mediated dark adaptation, is the earliest affected
354 and most persistent visual dysfunction in AMD (*6, 72*). Loss of RPE65 and CRALBP
355 immunoreactivity (without appearance of lipid droplets as in RPE65 deficiency (*73*))
356 suggests overall downregulation of a signature RPE function.
357 Our marker studies indicating RPE gain- and loss-of-function have implications for
358 therapeutic strategy. Molecular discovery in AMD is challenged by strong RPE
359 pigmentation and autofluorescence and the availability of donor eyes. Our finding of
360 reduced CRALBP immunoreactivity in abnormal RPE differs from a report of increased
361 CRALBP seen by 2-D gel electrophoresis (*74*). In the outer junctional zone of atrophy,
362 we previously showed vimentin immunoreactivity in enlarged RPE (*75*), suggestive of
363 epithelial-mesenchyme transition, and recently supported by increased Snail1 and
364 vimentin and decreased E-cadherin proteins in AMD eyes (*76, 77*) Cells in this transition
365 might be resistant to cell death, considered a positive feature (*76*), but they may also be
366 dysfunctional, according to our data. Other molecular RPE changes reported in AMD
367 (e.g., (*44, 74, 78-81*) are not yet localized to phenotypes translatable to clinical imaging.
368 Our evidence for molecular alteration in intact continuous RPE comports with re-
369 arrangement and loss of lipofuscin-attributable autofluorescence in geometrically precise

370 confluent cells (*82*). Therefore, a search for early interventions and preventative
371 measures for AMD is warranted.
372 Strengths of the clinical study are high-quality images and long follow-up on known
373 progression risk factors. Limitations include the small number of patients and lack of
374 independently assessed HFL trajectory. Strengths of the laboratory study are short post-
375 mortem specimens with attached retinas, comprehensive bright-field photomicroscopy to
376 visualize pigment, a color-contrasting readout for clear immunoreactivity signals, and a
377 cross-sectional format conducive to OCT comparison. Limitations include lack of clinical
378 records with pre-mortem imaging, lack of correlative data from flat mounts to show even
379 earlier RPE pathology, limited assessments of RPE adjacent to AMD deposits, and lack
380 of double-label experiments to determine cell-by-cell overlap among the four markers.
381 Nevertheless, this is most detailed characterization of RPE pathology in AMD to date in
382 either clinical or laboratory settings. HRF are one of the consensus OCT features for
383 AMD (*13*), encouraging longitudinal studies in other clinical centers. Our data can propel
384 new biomarker and therapeutic strategies for a common and currently untreatable cause
385 of impaired vision.
386

387 **MATERIALS AND METHODS**

388 **Study design, clinical imaging**

389 **Compliance**

390 Study of a clinical cohort and use of human tissue samples was approved by institutional
391 review board at Vitreous Macula Retina and University of Alabama at Birmingham,
392 respectively, and complied with the Health Insurance Portability and Accountability Act of
393 1996 and the Declaration of Helsinki.

394

395 **Patient selection, clinical image capture, and image analysis**

396 Consensus OCT nomenclature was used (*83*) in the context of a 3-layer Bruch's
397 membrane (*84*). The term RPE-basal lamina (RPE-BL) band was used for RPE
398 elevations from the inner collagenous layer of Bruch's membrane.

399 To analyze RPE plume natural history, patients with non-neovascular AMD on
400 OCT imaging seen by retinal specialist (authors KBF, LAY) at a tertiary private retinal
401 practice were retrospectively reviewed (author BL). Inclusion criteria included age over
402 50 years, more than 12 months of follow-up with tracked OCT B-scans at an inter-scan
403 spacing of ≤250 μm and maximum follow-up interval of 6 months, and at least one eye in
404 which HRF separated from and thought to originate from the RPE layer (i.e., if RPE-BL
405 thickness appeared reduced in a scan subsequent to HRF appearance). Patients with
406 diabetic retinopathy, retinal vascular disease, previous vitreoretinal surgery, laser
407 treatment or ocular inflammation were excluded. Eyes were evaluated at baseline by
408 presence of AMD lesions (soft, cuticular, subretinal drusenoid deposits, acquired
409 vitelliform lesion (*24*)), and if color fundus photographs were available, also pigmentary

410 changes. Presence of drusenoid pigment epithelial detachment (*85*) and cRORA (*12*)
411 was noted.
412 All patients underwent spectral domain OCT and near-infrared reflectance imaging
413 (Spectralis HRA + OCT, Heidelberg Engineering, Heidelberg, Germany) with eye
414 tracking enabled. The OCT protocol comprised 20° horizontal raster line scans centered
415 on the fovea (19 to 49 B-scans per eye; scan spacing at 115 to 250 µm, automatic real-
416 time averaging between 4 and 23).
417 Consecutive tracked OCT and near-infrared reflectance images were analyzed
418 over time and with reference to the foveal center, from the date of HRF appearance.
419 Plume morphology over time included nil change, change to a different morphology,
420 formation of an HRF with discrete reflective elements clearly separated from the RPE-BL
421 band, and dissolution. With the knowledge of the normal HFL architecture (fig. S2),
422 plume direction towards the OPL was noted as being congruent or incongruent with a
423 normal HFL architecture, i.e., parallel or non-parallel with curving fibers. Evolution of
424 underlying AMD pathology such as expansion of cRORA and drusen growth and
425 collapse were noted.
426
427 **Donor eye acquisition, ex vivo imaging, AMD diagnosis**
428 Whole eyes were obtained from deceased human donors (≥ 80 years of age, white, non-
429 diabetic, and ≤6 hours death-to-preservation) to the Advancing Sight Network
430 (Birmingham AL USA) during 2016-17. Pre-mortem eye health history was not available.
431 Eyes were preserved in 4% buffered paraformaldehyde and screened for AMD presence
432 and stage using *ex vivo* multimodal imaging including OCT, as described, (*20*) and
433 stored in 1% buffered paraformaldehyde at 4°C until used. This study used 16 AMD

434 eyes (7 early-intermediate AMD, 6 atrophic AMD, 3 neovascular AMD) and 4 age-
435 matched control eyes (table S5).
436 Rectangles of full-thickness eye wall (5x8 mm) including fovea and optic nerve
437 were dissected. To prevent ice crystals, tissue was cryoprotected in ascending
438 concentrations of sucrose in phosphate buffered saline (PBS) then ascending
439 concentrations of tissue embedding medium and sucrose buffer (HistoPrep, Thermo
440 Fisher Scientific, #SH75-1250D, Rockford IL USA); 4 parts sucrose buffer and 1part
441 medium then 2:1 sucrose: medium. Tissue was placed into a cryomold (Electron
442 Microscopy Sciences, #70176-10, Fort Washington PA USA) with embedding medium,
443 oriented, frozen in liquid nitrogen, and stored at -80°C. Tissues were sectioned at 12 μm
444 thickness on a cryostat (Leica CM3050 Vashaw Scientific, Norcross GA USA), air dried
445 at 37°C overnight, and stored at -80°C until used.
446 For AMD diagnosis and imaging-histology correlation, cryosections through the
447 fovea and perifovea (recognized by HFL) were stained with periodic acid Schiff
448 hematoxylin to highlight Bruch's membrane and sub-RPE deposits. One stained section
449 per slide was scanned with a 20X objective and a robotic microscope stage (Olympus
450 VSI 120, CellSens; Olympus, Center Valley PA), scaled to tissue units, and centered on
451 the fovea or vertical meridian (where Henle fibers diverge) using a custom plugin for FIJI
452 (https://imagej.nih.gov/ij/download.html). *Ex vivo* OCT B-scans and scanned whole
453 sections were matched for major landmarks (e.g., overall tissue contour, foveal center,
454 large vessels, individual pathologies). For figures, images were adjusted to maximize the
455 intensity histogram for contrast and white balance and made into composites
456 (Photoshop CS6, Adobe Systems, USA).
457

458 **Immunohistochemistry and evaluation**

459 Markers for retinoid activity and immune function were localized in cells of RPE origin
460 (*86*) sections processed with an avidin-biotin-peroxidase immunohistochemistry
461 detection system and antibodies list in table S6. Cryosections were warmed, hydrated in
462 PBS at room temperature, and processed for 15 minutes under steam with an antigen
463 retrieval solution (Vector Labs, #H-3300-250) in glycerol. Quenched endogenous
464 hydrogen peroxide with 3% H_2O_2 diluted from 30% H_2O_2 (Thermo Fisher Scientific
465 Cat# H-325-100) with distilled H_2O for ten minutes at room temperature (except for
466 CD68 after primary antibody as manufacture mentioned). Non-specific binding was
467 blocked with 5% horse serum for 1 hour at room temperature, then incubated with
468 primary antibodies of mouse anti-CD68, CD163, RPE65, or CRALBP at 4ºC for 40
469 hours. Following PBS wash, sections were incubated with avidin and biotin solutions for
470 15 minutes respectively, washed (x3), then incubated with horse anti-mouse secondary
471 antibody (Vector Labs Vectastain Elite ABC Kit RTU Universal, #PK-7200) for 4 hours at
472 room temperature, washed (x3), and incubated with ABC complex solution (Vector Labs
473 Vectastain Elite ABC Kit RTU Universal, #PK-7200) for 30 minutes at room temperature,
474 and washed. A red reaction product was developed with Vector AEC Peroxidase
475 Substrate Kit (Vector Labs, Burlingame CA USA #SK-4200) to the desired color (~30
476 minutes). After washing with distilled water (5 minutes x 3), sections were counterstained
477 with hematoxylin solution for 5 minutes followed by 20 seconds bluing solution (Poly
478 Scientific R&D Corp, Bay Shore NY USA; #S127-160Z) then washed. Coverslips were
479 mounted with aqueous medium (VectaMount AQ, Vector Labs, #H-5501-60) and sealed
480 with nail polish, air-dried, and stored at 4ºC. As shown in fig. S7, we used isotype-

481 specific negative controls (mouse antibodies), sham controls omitting primary antibody,
482 and external and internal positive controls.
483 Glass slides were scanned using the system described above and 20x and 40x
484 objectives. RPE phenotype was categorized using the Project MACULA grading system.
485 (*18, 19*) In each stained section (1 per antibody per eye), immunoreactivities for each
486 RPE phenotype were scored semi-quantitatively by a single observer (author DC after
487 training by author CAC) as 0-not stained, 1-some stained and 2- all stained. These
488 scores were converted to percentages (fig. S9) using by total scores of eyes for each
489 phenotype divided by maximum score (2 x number of eyes with the phenotype) times
490 100. Each phenotype was seen in at least 3 eyes.
491

492 **SUPPLEMENTARY MATERIALS**

493 **Supplementary figures**

494 Fig. S1. A path from hyperreflective foci (HRF) to complete retinal pigment epithelium
495 (RPE) and outer retinal atrophy (cRORA) in AMD.
496 Fig. S2. Henle fibers in the human macula.
497 Fig. S3. Retinal pigment epithelium plumes exhibit directionality
498 Fig. S4. Duration and evolution of plumes
499 Fig. S5. Variations in RPE plume trajectory in atrophy.
500 Fig. S6. HRF in ex vivo OCT match intraretinal RPE on histology
501 Fig. S7. Positive and negative controls for immunohistochemistry
502 Fig. S8: RPE corresponding to HRF and other abnormal cells are CD163+
503 Fig. S9. Gain- and loss-of-function of RPE and RPE-derived cells
504 Fig. S10. Dispersing melanosomes follow regionally specific trajectories of Müller glia

505 **Supplementary tables**

506 Table S1. Demographics of clinic patients

507 Table S2. Plume disposition at final visit

508 Table S3. Plume trajectory relative to HFL and macular quadrant

509 Table S4. Plume association with atrophy

510 Table S5. Characteristics of donor eyes

511 Table S6. Antibodies used

512 Table S7. Morphologic phenotypes of RPE and its basal lamina in AMD

513

514

515

Acknowledgments

We thank Advancing Sight Network (formerly the Alabama Eye Bank) for timely retrieval of donor eyes and David Fisher for graphics in Supplementary Figure 1.

Funding

This work was supported by National Institutes of Health (Bethesda, MD, USA) grant R01EY015520 (CAC); The Macula Foundation, Inc., New York, NY; an anonymous donor to AMD research at UAB; unrestricted funds to the Department of Ophthalmology from Research to Prevent Blindness, Inc.; and EyeSight Foundation of Alabama. Acquisition of human tissues for immunohistochemistry was funded by NIH grant R01EY015520 (CAC) and R01EY027948 (CAC, TA) and IZKF Würzburg (N-304, TA).

Author contributions

C.A.C. designed, supervised study and wrote the manuscript. D.C. designed and performed immunohistochemistry experiments. B.L. designed and conducted clinical studies and wrote the manuscript. J.M. conducted *ex vivo* imaging, tissue cryosections, and microscopy. D.K. made Fig. S2. T.A. edited manuscript. L.A.Y. and K.B.F designed and supervised clinical study. K.B.F. edited manuscript. C.A.C. and T.A. raised funding.

Competing interests

T.A. receives research funding from Novartis and is a stockholder of MacRegen Inc. K.B.F. is a consultant to Genentech, Optovue, Zeiss, Heidelberg Engineering, Allergan, and Novartis. C.A.C. receives research funds from Genentech/ Hoffman LaRoche and Heidelberg Engineering and is a stockholder of MacRegen Inc.

Data and materials availability

All other data associated with this study are present in the paper or the Supplementary Materials. Materials are available upon request from the corresponding author.

541 **Figures and Captions**

542 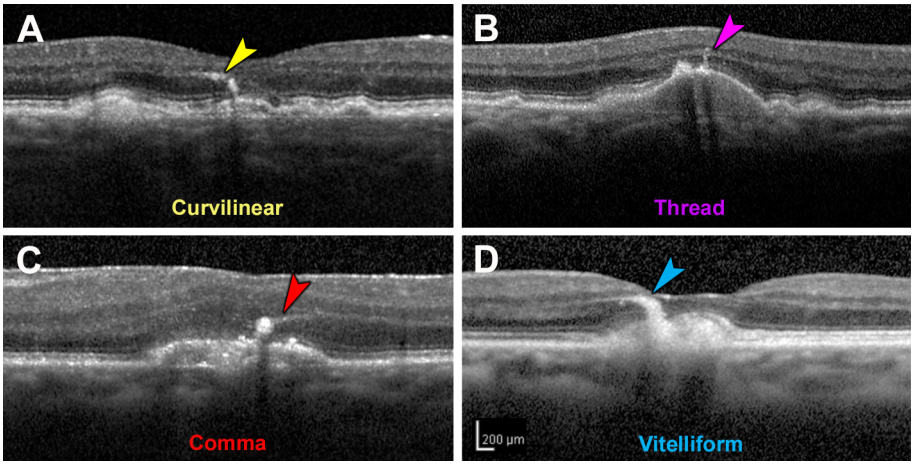

543 **Fig. 1**. **Morphology of retinal pigment epithelium plumes.**

544 Examples from two eyes of one patient. (**A**) “Curvilinear” consists of hyperreflective
545 structures of consistent width, often arising from a soft druse and aiming towards the
546 outer plexiform layer. (**B**) “Thread” has a uniform and thin width, compared to
547 Curvilinear. (**C**) “Comma” has a wide base adjacent to the RPE layer and an anterior
548 taper. (**D**) “Vitelliform” is thick and arises from an acquired vitelliform lesion (*24*).

549

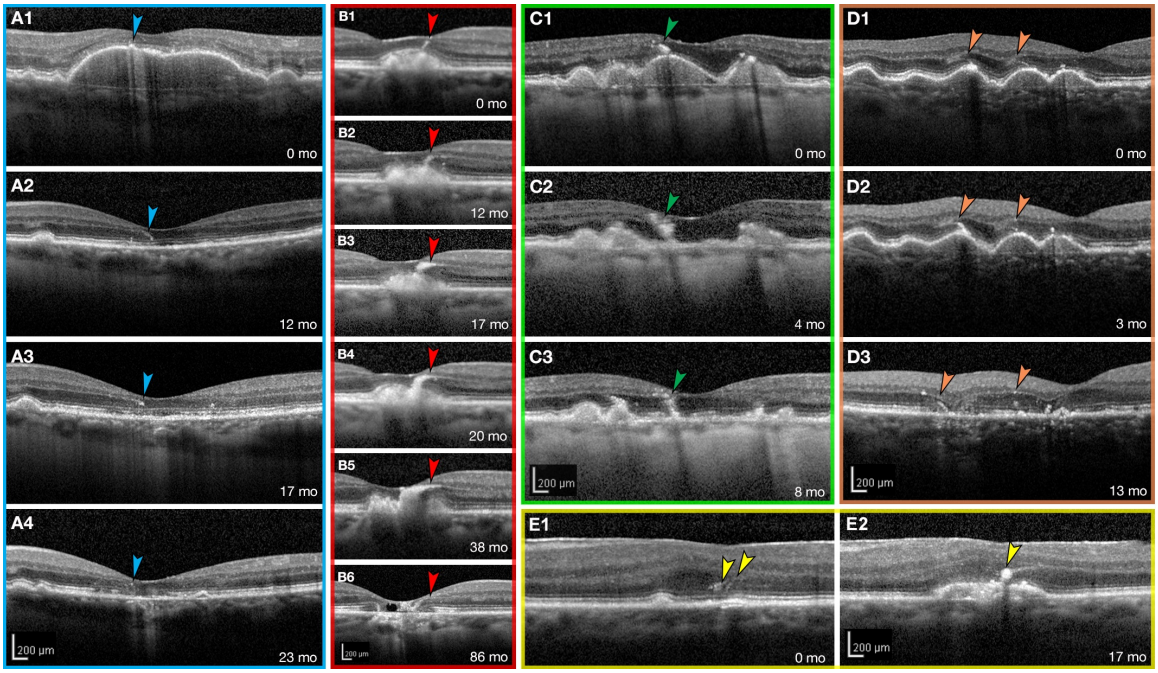

Fig. 2. **Retinal pigment epithelium plumes evolve over time.**

(**A** to **E**) Tracked optical coherence tomography B-scans of 5 different eyes with AMD are shown with individualized colored frames and scale bars. Numbers in the lower right corners indicate time elapsed in months since the baseline visit at 0 months. (**A1** to **A4**) Hyperreflective foci (HRF) overlie a drusenoid pigment epithelial detachment that collapsed at 12 months. HRF evolve into a comma plume before disappearing into complete outer retinal atrophy (cORA (*12*)). (**B1** to **B6**) A curvilinear plume evolves into a vitelliform plume, which collapses, leaving atrophy and degenerative cysts. (**C1** to **C3)** A comma-type plume evolves into HRF upon drusen collapse. (**D1** to **D3**) Of two thread plumes at baseline, one (left) becomes curvilinear at 3 months and persists through drusen collapse and *incomplete* RPE and outer retinal atrophy at 13 months. Thread plume at the right has disappeared at 13 months. (**E1** to **E2**)**.** Two thread plumes evolve into a comma plume as an RPE elevation appears. This eye also has an epiretinal membrane.

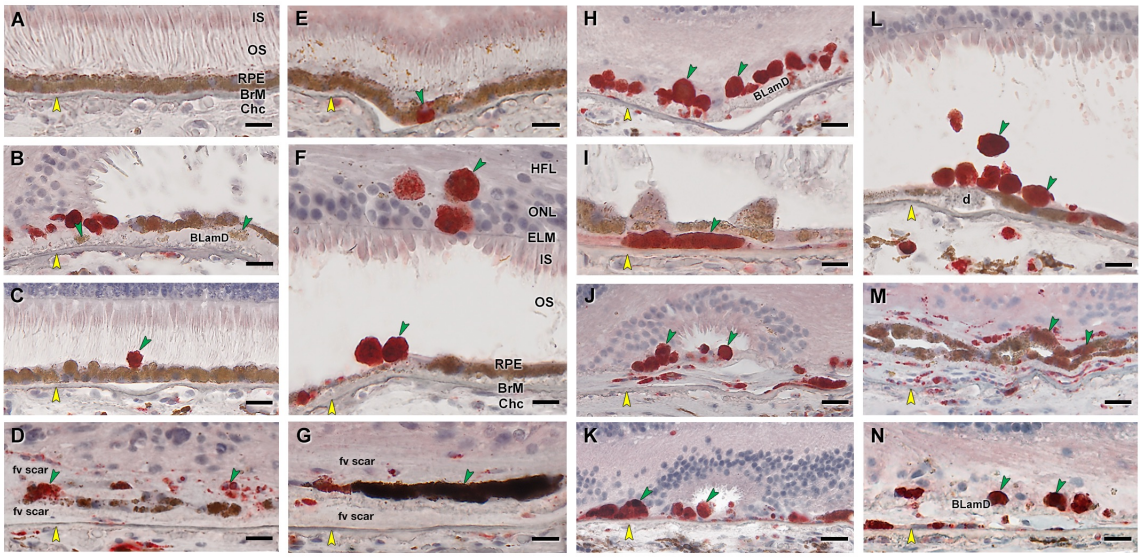

Fig. 3. RPE corresponding to HRF and other abnormal cells are CD68+. Twenty donor eyes (16 AMD, 4 control; eye numbers in table S5) were used for immunohistochemistry with mouse monoclonal anti-human CD68 (table S6). Fourteen of 16 previously described morphologic phenotypes of RPE (*25*) were identified (table S7). All scale bars are 20 μm; yellow arrowheads indicate BrM, and green arrowheads indicate abnormal phenotypes. (**A**) CD68- "Uniform" RPE, unremarkable (#1). (**B**) CD68- granule aggregates, released basally from ''Shedding'' RPE; atrophic AMD (#13). (**C**) CD68+ ''Sloughed'' RPE; atrophic AMD (#12). **D.** Both CD68+ and CD68- ''Entombed'' RPE; nvAMD (#18). (**C**) A single CD68+ "Nonuniform" RPE from a less-affected area, nvAMD (#20). (**F**) CD68+ ''Intraretinal'' RPE; early-intermediate AMD (#7). (**G**) Variable CD68 immunoreactivity in ''Melanotic'' RPE, nvAMD (#18). CD68 immunoreactivity is variable on heavily and light pigmented melanotic RPE. **H.** CD68+ "Severe" RPE; atrophic AMD (#13). (**I**) CD68+ ''Subducted'' RPE, atrophic AMD (#12). (**J**) CD68+ ''Entubulated'' RPE, atrophic AMD (#12). (**K)** CD68+ ''Dissociated'' RPE, atrophic AMD (#12). (**L**) CD68+ "Dissociated" RPE and "Sloughed" RPE, early-intermediate AMD (#7).

582 (**M**) Variable CD68 immunoreactivity in ‘‘Bilaminar’’ RPE, nvAMD (#20). (**N**) CD68+

583 “Dissociated” RPE; atrophic AMD (#12).

584

585

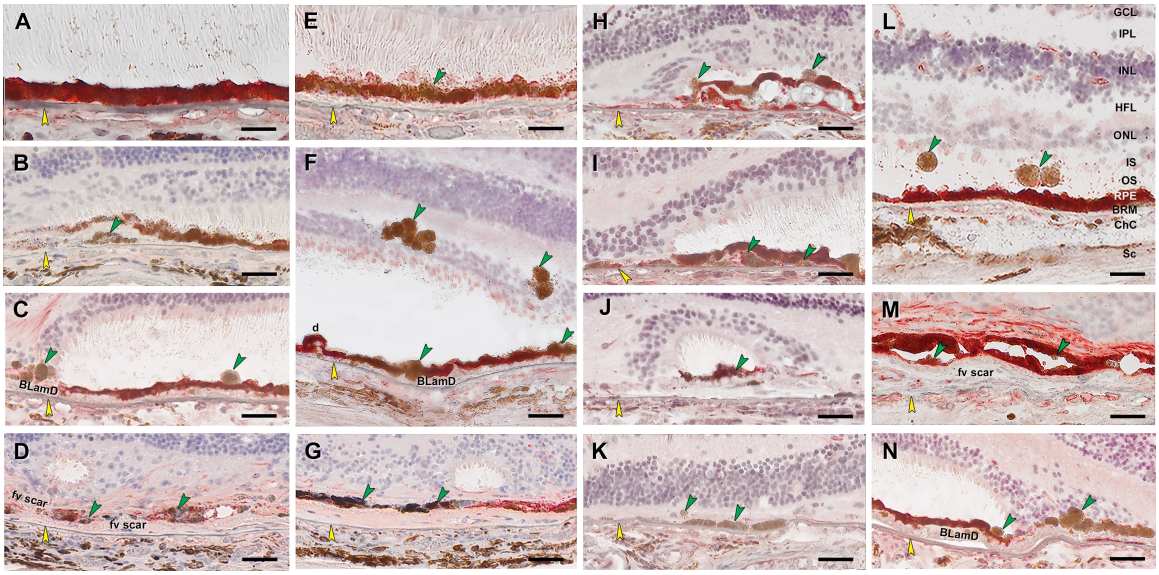

Fig. 4. RPE corresponding to HRF and other abnormal cells are RPE65-.

Twenty donor eyes (16 AMD, 4 control; eye numbers in table S5) were for immunohistochemistry with mouse monoclonal anti-human RPE65 (table S6). Fourteen of 16 previously described morphologic phenotypes of RPE were identified (table S7). All scale bars are 20 μm; yellow arrowheads indicate BrM; green arrowheads indicate abnormal RPE phenotypes. (**A**) RPE65+ “Uniform” RPE, unremarkable (#1). (**B**) RPE65- ‘‘Shedding’’ RPE, nvAMD (#20). (**C**) RPE65- ‘‘Sloughed’’ RPE, atrophic AMD (#13). (**D**) Both RPE65+ and REP65- ‘‘Entombed’’ RPE, nvAMD (#18). (**E**) A few RPE65- “Nonuniform” RPE, early-intermediate AMD (#6). (**F**) RPE65- ‘‘Intraretinal’’ RPE, early-intermediate AMD (#11). (**G**) Variable RPE65 immunoreactive ‘‘Melanotic’’ RPE, nvAMD (#18). (**H**) RPE65- “Severe” RPE, atrophic AMD (#12). (**I**) RPE65- ‘‘Subducted’’ RPE, atrophic AMD (#12). (**J**) Both RPE65+ and RPE65- ‘‘Entubulated’’ RPE, atrophic AMD (#12). (**K**) RPE65- RPE at ‘‘Atrophy without BLamD’’ area, atrophic AMD (#12). (**L**) RPE65- “Dissociated” RPE, atrophic AMD (#16). (**M**) Both RPE65- and RPE65+

601 ‘‘Bilaminar’’ RPE, nvAMD (#20). (**N**) RPE65- RPE at ‘‘Atrophy with BLamD’’ area,

602 atrophic AMD eye (#13).

603

604

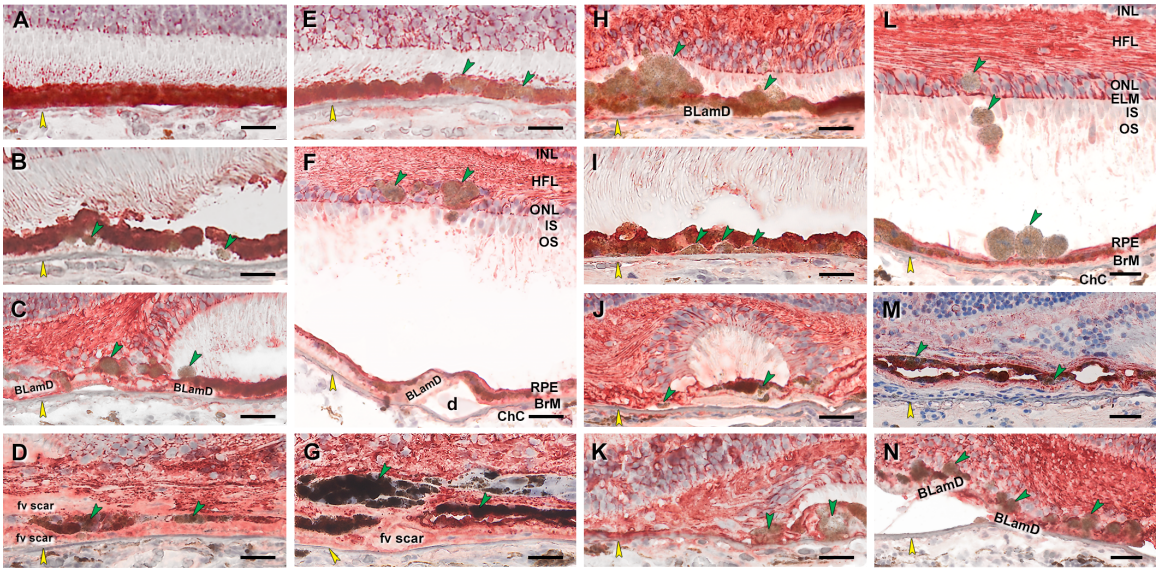

Fig. 5. Abnormal RPE is CRALBP-, Müller glia are CRALBP+.

Twenty donor eyes (16 AMD, 4 control; eye numbers in table S5) were used for immunohistochemistry with mouse monoclonal anti-human CRALBP (table S6). Fourteen of 16 previously described morphologic phenotypes of RPE were identified (table S7). All scale bars are 20 μm. Yellow arrowheads indicate BrM. Green arrowheads indicate abnormal phenotypes including migrating RPE corresponding to HRF. (A) CRALBP+ “Uniform” RPE, unremarkable (#1). (B) CRALBP- ‘‘Shedding’’ RPE, early-intermediate AMD (#6). (C) CRALBP- ‘‘Sloughed’’ RPE, atrophic AMD (#13). (D) Both CRALBP+ and CRALBP- ‘‘Entombed’’ RPE nvAMD (#18). (E)CRALBP- “Nonuniform” RPE nvAMD (#18). (F) CRALBP- ‘‘Intraretinal’’ RPE, early-intermediate AMD eye (#7). (G) Both CRALBP+ and CRALBP- ‘‘Melanotic’’ RPE, nvAMD (#18). (H) CRALBP- “Severe” RPE, atrophic AMD (#12). (I) CRALBP- ‘‘Subducted’’ RPE, atrophic AMD (#12). (J) Both CRALBP+ and CRALBP- ‘‘Entubulated’’ RPE, atrophic AMD (#12). (K) CRALBP- RPE at ‘‘Atrophy without BLamD’’ area, atrophic AMD (#12). (L) CRALBP- “Dissociated” RPE, early-intermediate AMD (#7). (M) Variable CRALBP

621 immunoreactivity in ‘‘Bilaminar’’ RPE, nvAMD (#20). (N) Variable CRALBP+ and

622 CRALBP- RPE at ‘‘Atrophy with BLamD’’ area, nvAMD (#7).

623

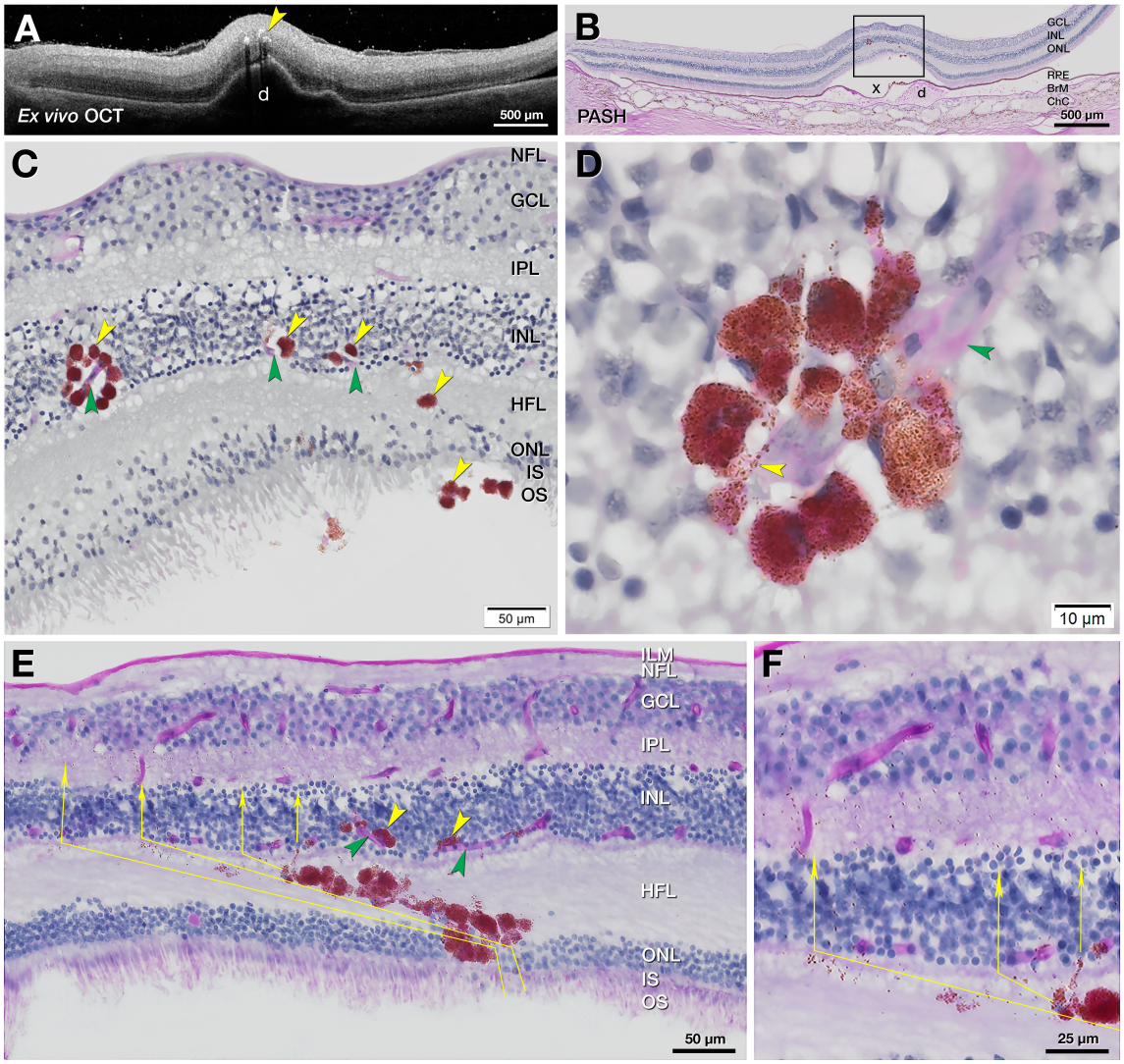

Fig. 6. RPE migrate toward vessels and follow Müller glial columns.

One eye from each of two donors aged 86-90 years (#5 and #15, table S5) were subjected to *ex vivo* OCT images in A (fig. S6, C1 and C2) and PASH staining with cryosections in B, E and F. (**A**) *Ex vivo* OCT of donor eye (#5) shows HRF (yellow arrowhead) over a large druse. (**B**) Corresponding PASH histologic section 290 µm superior to the fovea with a big druse (d), artifactually detached (x) from the RPE, and thinner ONL. (**C**) Magnified RPE rosette in B (yellow arrowheads) crossing the HFL and

633 approaching retinal capillaries (green arrowheads). (**D**) Nucleated RPE rosette from
634 panel C (adjacent section). RPE-characteristic spindle-shaped melanosomes and
635 melanolipofuscin impart a brown hue. The surrounded capillary is stained light pink
636 (green arrowhead) with endothelial cell nuclei. Processes containing RPE organelles
637 extend along the capillaries. (**E** and **F**) In another plume, RPE cells and detritus take a Z-
638 shaped course. Fully pigmented RPE cells cross the obliquely oriented fibers of the HFL,
639 with individual and grouped organelles in the lead (thin yellow arrows). The path turns
640 vertically to enter and cross the INL and IPL.
641

642 **References**

643 1. S. R. Flaxman, R. R. A. Bourne, S. Resnikoff, P. Ackland, T. Braithwaite, M. V.
644 Cicinelli, A. Das, J. B. Jonas, J. Keeffe, J. H. Kempen, J. Leasher, H. Limburg, K.
645 Naidoo, K. Pesudovs, A. Silvester, G. A. Stevens, N. Tahhan, T. Y. Wong, H. R. Taylor,
646 S. Vision Loss Expert Group of the Global Burden of Disease, Global causes of
647 blindness and distance vision impairment 1990-2020: a systematic review and meta-
648 analysis. *The Lancet. Global health* 5, e1221-e1234 (2017).
649 2. M. G. Maguire, D. F. Martin, G. S. Ying, G. J. Jaffe, E. Daniel, J. E. Grunwald, C.
650 A. Toth, F. L. Ferris, 3rd, S. L. Fine, Five-year outcomes with anti-vascular endothelial
651 growth factor treatment of neovascular age-related macular degeneration: the
652 Comparison of Age-Related Macular Degeneration Treatments Trials. *Ophthalmology*
653 123, 1751-1761 (2016).
654 3. L. Chen, J. D. Messinger, D. Kar, J. L. Duncan, C. A. Curcio, Biometrics, impact,
655 and significance of basal linear deposit and subretinal drusenoid deposit in age-related
656 macular degeneration. *Invest. Ophthalmol. Vis. Sci.* 62, 33 (2021).
657 4. P. A. Keane, P. J. Patel, S. Liakopoulos, F. M. Heussen, S. R. Sadda, A. Tufail,
658 Evaluation of age-related macular degeneration with optical coherence tomography.
659 *Surv Ophthalmol* 57, 389-414 (2012).
660 5. R. H. Guymer, P. J. Rosenfeld, C. A. Curcio, F. G. Holz, G. Staurenghi, K. B.
661 Freund, S. Schmitz-Valckenberg, J. R. Sparrow, R. F. Spaide, A. Tufail, U.
662 Chakravarthy, G. J. Jaffe, K. Csaky, D. Sarraf, J. M. Monés, R. Tadayoni, J. Grunwald,
663 F. Bottoni, S. Liakopoulos, D. Pauleikhoff, S. Pagliarini, E. Y. Chew, F. Viola, M.
664 Fleckenstein, B. Blodi, T. H. Lim, V. Chong, G. A. Lutty, A. C. Bird, S. R. Sadda,
665 Incomplete retinal pigment epithelial and outer retinal atrophy (iRORA) in age-related
666 macular degeneration: CAM Report 4. *Ophthalmology* 127, 394-409 (2020).
667 6. C. Owsley, G. McGwin, Jr., M. E. Clark, G. R. Jackson, M. A. Callahan, L. B. Kline,
668 C. D. Witherspoon, C. A. Curcio, Delayed rod-mediated dark adaptation is a functional
669 biomarker for incident early age-related macular degeneration. *Ophthalmology* 123, 344-
670 351 (2016).
671 7. T. D. Lamb, E. N. Pugh, Jr., Phototransduction, dark adaptation, and rhodopsin
672 regeneration: the Proctor Lecture. *Invest Ophthalmol Vis Sci* 47, 5137-5152 (2006).
673 8. J. C. Saari, Vitamin A and Vision. *Subcell Biochem* 81, 231-259 (2016).
674 9. A. Pollreisz, M. Neschi, K. R. Sloan, M. Pircher, T. J. Mittermueller, D. M. Dacey,
675 U. Schmidt-Erfurth, C. A. Curcio, An atlas of human retinal pigment epithelium
676 organelles significant for clinical imaging. *Invest Ophthalmol Vis Sci* 61, 13 (2020).
677 10. M. Li, C. Huisingh, J. D. Messinger, R. Dolz-Marco, D. Ferrara, K. B. Freund, C. A.
678 Curcio, Histology of geographic atrophy secondary to age-related macular degeneration:
679 a multilayer approach. *Retina* 38, 1937-1953 (2018).
680 11. F. G. Holz, S. Sadda, G. Staurenghi, M. Lindner, A. C. Bird, B. A. Blodi, B. Bottoni,
681 U. Chakravarthy, E. Chew, K. Csaky, C. A. Curcio, R. Danis, K. B. Freund, J. Grunwald,
682 R. Guymer, C. Hoyng, G. J. Jaffe, S. Liakopoulos, J. Monés, A. Oishi, D. Pauleikhoff, P.
683 J. Rosenfeld, D. Sarraf, R. F. Spaide, R. Tadayoni, A. Tufail, S. Wolf, S. Schmitz-
684 Valckenberg, Imaging protocols for clinical studies in age-related macular degeneration
685 – recommendations from Classification of Atrophy (CAM) Consensus Meeting.
686 *Ophthalmology* 124, 464-478 (2017).
687 12. S. R. Sadda, R. Guymer, F. G. Holz, S. Schmitz-Valckenberg, C. A. Curcio, A. C.
688 Bird, B. A. Blodi, F. Bottoni, U. Chakravarthy, E. Y. Chew, K. Csaky, R. Danis, M.

Fleckenstein, K. B. Freund, J. Grunwald, C. B. Hoyng, G. J. Jaffe, S. Liakopoulos, J. Monés, D. Pauleikhoff, P. J. Rosenfeld, D. Sarraf, R. F. Spaide, R. Tadayoni, A. Tufail, S. Wolf, G. Staurenghi, Consensus definition for atrophy associated with age-related macular degeneration on optical coherence tomography: CAM Report 3. *Ophthalmology* 125, 537-548 (2018).

13. G. J. Jaffe, U. Chakravarthy, K. B. Freund, R. H. Guymer, F. G. Holz, S. Liakopoulos, J. Monés, P. J. Rosenfeld, S. R. Sadda, D. Sarraf, S. Schmitz-Valckenberg, R. F. Spaide, G. Staurenghi, A. Tufail, C. A. Curcio, Imaging features associated with progression to geographic atrophy in age-related macular degeneration: CAM Report 5. *Ophthalmology Retina* 12/20/20 online, (2020).

14. Y. Ouyang, F. M. Heussen, A. Hariri, P. A. Keane, S. R. Sadda, Optical coherence tomography-based observation of the natural history of drusenoid lesion in eyes with dry age-related macular degeneration. *Ophthalmology* 120, 2656-2665 (2013).

15. J. G. Christenbury, F. A. Folgar, R. V. O'Connell, S. J. Chiu, S. Farsiu, C. A. Toth, Progression of intermediate age-related macular degeneration with proliferation and inner retinal migration of hyperreflective foci. *Ophthalmology* 120, 1038-1045 (2013).

16. M. Nassisi, J. Lei, N. S. Abdelfattah, A. Karamat, S. Balasubramanian, W. Fan, A. Uji, K. M. Marion, K. Baker, X. Huang, E. Morgenthien, S. R. Sadda, OCT risk factors for development of late age-related macular degeneration in the fellow eyes of patients enrolled in the HARBOR study. *Ophthalmology* 126, 1667-1674 (2019).

17. S. M. Waldstein, W.-D. Vogl, H. Bogunovic, A. Sadeghipour, S. Riedl, U. Schmidt-Erfurth, Characterization of drusen and hyperreflective foci as biomarkers for disease progression in age-related macular degeneration using artificial intelligence in optical coherence tomography. *JAMA Ophthalmology* 138, 740-747 (2020).

18. E. C. Zanzottera, J. D. Messinger, T. Ach, R. T. Smith, K. B. Freund, C. A. Curcio, The Project MACULA retinal pigment epithelium grading system for histology and optical coherence tomography in age-related macular degeneration. *Invest Ophthalmol Vis Sci* 56, 3253-3268 (2015).

19. E. C. Zanzottera, J. D. Messinger, T. Ach, R. T. Smith, C. A. Curcio, Subducted and Melanotic cells in advanced age-related macular degeneration are derived from retinal pigment epithelium. *Invest Ophthalmol Vis Sci* 56, 3269-3278 (2015).

20. C. Balaratnasingam, J. D. Messinger, K. R. Sloan, L. A. Yannuzzi, K. B. Freund, C. A. Curcio, Histologic and optical coherence tomographic correlations in drusenoid pigment epithelium detachment in age-related macular degeneration. *Ophthalmology* 124, 644-656 (2017).

21. M. Li, R. Dolz-Marco, J. D. Messinger, L. Wang, R. M. Feist, C. A. Girkin, S. Gattoussi, D. Ferrara, C. A. Curcio, K. B. Freund, Clinicopathologic correlation of anti-vascular endothelial growth factor-treated type 3 neovascularization in age-related macular degeneration. *Ophthalmology* 125, 276-287 (2018).

22. C. Jopling, S. Boue, J. C. Izpisua Belmonte, Dedifferentiation, transdifferentiation and reprogramming: three routes to regeneration. *Nat Rev Mol Cell Biol* 12, 79-89 (2011).

23. J. R. Sparrow, M. Marsiglia, R. Allikmets, S. Tsang, W. Lee, T. Duncker, J. Zernant, Flecks in recessive Stargardt disease: short-wavelength autofluorescence, near-infrared autofluorescence, and optical coherence tomography. *Invest Ophthalmol Vis Sci* 56, 5029-5039 (2015).

735 24. K. B. Freund, K. Laud, L. H. Lima, R. F. Spaide, S. Zweifel, L. A. Yannuzzi,
736 Acquired vitelliform lesions: correlation of clinical findings and multiple imaging analyses.
737 *Retina* 31, 13-25 (2011).
738 25. C. A. Curcio, E. C. Zanzottera, T. Ach, C. Balaratnasingam, K. B. Freund,
739 Activated retinal pigment epithelium, an optical coherence tomography biomarker for
740 progression in age-related macular degeneration. *Invest Ophthalmol Vis Sci* 58, BIO211-
741 BIO226 (2017).
742 26. M. H. Barros, F. Hauck, J. H. Dreyer, B. Kempkes, G. Niedobitek, Macrophage
743 polarisation: an immunohistochemical approach for identifying M1 and M2 macrophages.
744 *PLoS One* 8, e80908 (2013).
745 27. D. A. Chistiakov, M. C. Killingsworth, V. A. Myasoedova, A. N. Orekhov, Y. V.
746 Bobryshev, CD68/macrosialin: not just a histochemical marker. *Lab Invest* 97, 4-13
747 (2017).
748 28. K. B. Schaal, K. B. Freund, K. M. Litts, Y. Zhang, J. D. Messinger, C. A. Curcio,
749 Outer retinal tubulation in advanced age-related macular degeneration: optical
750 coherence tomographic findings correspond to histology. *Retina* 35, 1339-1350 (2015).
751 29. A. Etzerodt, S. K. Moestrup, CD163 and inflammation: biological, diagnostic, and
752 therapeutic aspects. *Antioxid Redox Signal* 18, 2352-2363 (2013).
753 30. M. Karlstetter, R. Scholz, M. Rutar, W. T. Wong, J. M. Provis, T. Langmann,
754 Retinal microglia: just bystander or target for therapy? *Prog Retin Eye Res* 45, 30-57
755 (2015).
756 31. E. M. Lad, S. W. Cousins, A. D. Proia, Identity of pigmented subretinal cells in age-
757 related macular degeneration. *Graefes Arch Clin Exp Ophthalmol* 254, 1239-1241
758 (2016).
759 32. M. A. Margeta, E. M. Lad, A. D. Proia, CD163+ macrophages infiltrate axon
760 bundles of postmortem optic nerves with glaucoma. *Graefes Arch Clin Exp Ophthalmol*
761 256, 2449-2456 (2018).
762 33. J. von Lintig, J. Moon, D. Babino, Molecular components affecting ocular
763 carotenoid and retinoid homeostasis. *Prog Retin Eye Res* 80, 100864 (2021).
764 34. Y. Xue, S. Q. Shen, J. Jui, A. C. Rupp, L. C. Byrne, S. Hattar, J. G. Flannery, J. C.
765 Corbo, V. J. Kefalov, CRALBP supports the mammalian retinal visual cycle and cone
766 vision. *J Clin Invest* 125, 727-738 (2015).
767 35. T. Liu, E. Jenwitheesuk, D. C. Teller, R. Samudrala, Structural insights into the
768 cellular retinaldehyde-binding protein (CRALBP). *Proteins* 61, 412-422 (2005).
769 36. T. Ach, E. Tolstik, J. D. Messinger, A. V. Zarubina, R. Heintzmann, C. A. Curcio,
770 Lipofuscin re-distribution and loss accompanied by cytoskeletal stress in retinal pigment
771 epithelium of eyes with age-related macular degeneration. *Invest Ophthalmol Vis Sci* 56,
772 3242-3252 (2015).
773 37. S. Omri, B. Omri, M. Savoldelli, L. Jonet, B. Thillaye-Goldenberg, G. Thuret, P.
774 Gain, J. C. Jeanny, P. Crisanti, F. Behar-Cohen, The outer limiting membrane (OLM)
775 revisited: clinical implications. *Clin Ophthalmol* 4, 183-195 (2010).
776 38. E. C. Zanzottera, T. Ach, C. Huisingh, J. D. Messinger, R. F. Spaide, C. A. Curcio,
777 Visualizing retinal pigment epithelium phenotypes in the transition to geographic atrophy
778 in age-related macular degeneration. *Retina* 36 Suppl 1, S12-S25 (2016).
779 39. A. Matet, M. C. Savastano, M. Rispoli, C. Bergin, A. Moulin, P. Crisanti, F. Behar-
780 Cohen, B. Lumbroso, En face optical coherence tomography of foveal microstructure in
781 full-thickness macular hole: a model to study perifoveal Muller cells. *Am J Ophthalmol*
782 159, 1142-1151 e1143 (2015).

783 40. F. L. Ferris, 3rd, C. P. Wilkinson, A. Bird, U. Chakravarthy, E. Chew, K. Csaky, S.
784 R. Sadda, Clinical classification of age-related macular degeneration. *Ophthalmology*
785 120, 844-851 (2013).
786 41. J. Lei, S. Balasubramanian, N. S. Abdelfattah, M. Nittala, S. R. Sadda, Proposal of
787 a simple optical coherence tomography-based scoring system for progression of age
788 related macular degeneration. *Graefes Arch Clin Exp Ophthalmol* 255, 1551-1558
789 (2017).
790 42. U. Nicolai, C. Eckardt, The occurrence of macrophages in the retina and periretinal
791 tissues in ocular diseases. *Ger J Ophthalmol* 2, 195-201 (1993).
792 43. V. L. Bonilha, B. A. Bell, J. Hu, C. Milliner, G. J. Pauer, S. A. Hagstrom, R. A.
793 Radu, J. G. Hollyfield, Geographic atrophy: confocal scanning laser ophthalmoscopy,
794 histology, and inflammation in the region of expanding lesions. *Invest Ophthalmol Vis Sci*
795 61, 15 (2020).
796 44. J. A. Matsubara, Y. Tian, J. Z. Cui, M. R. Zeglinski, S. Hiroyasu, C. T. Turner, D. J.
797 Granville, Retinal distribution and extracellular activity of granzyme B: a serine protease
798 that degrades retinal pigment epithelial tight junctions and extracellular matrix proteins.
799 *Front Immunol* 11, 574 (2020).
800 45. K. C. Chen, J. J. Jung, C. A. Curcio, C. Balaratnasingam, R. Gallego-Pinazo, R.
801 Dolz-Marco, K. B. Freund, L. A. Yannuzzi, Intraretinal hyperreflective foci in acquired
802 vitelliform lesions of the macula: clinical and histologic study. *Am J Ophthalmol* 164, 89-
803 98 (2016).
804 46. S. Cherepanoff, P. G. McMenamin, M. C. Gillies, E. Kettle, S. H. Sarks, Bruch's
805 membrane and choroidal macrophages in early and advanced age-related macular
806 degeneration. *Br J Ophthalmol* 94, 918-925 (2010).
807 47. D. S. McLeod, I. Bhutto, M. M. Edwards, R. E. Silver, J. M. Seddon, G. A. Lutty,
808 Distribution and quantification of choroidal macrophages in human eyes with age-related
809 macular degeneration. *Invest Ophthalmol Vis Sci* 57, 5843-5855 (2016).
810 48. S. G. Elner, V. M. Elner, J. C. Nielsen, E. Torczynski, R. Yu, W. A. Franklin, CD68
811 antigen expression by human retinal pigment epithelial cells. *Exp Eye Res* 55, 21-28.
812 (1992).
813 49. O. Tatar, E. Yoeruek, P. Szurman, K. U. Bartz-Schmidt, G. Tubingen Bevacizumab
814 Study, A. Adam, K. Shinoda, C. Eckardt, V. Boeyden, C. Claes, G. Pertile, G. B.
815 Scharioth, S. Grisanti, Effect of bevacizumab on inflammation and proliferation in human
816 choroidal neovascularization. *Arch Ophthalmol* 126, 782-790 (2008).
817 50. C. M. Sheridan, S. Pate, P. Hiscott, D. Wong, D. M. Pattwell, D. Kent, Expression
818 of hypoxia-inducible factor-1alpha and -2alpha in human choroidal neovascular
819 membranes. *Graefes Arch Clin Exp Ophthalmol* 247, 1361-1367 (2009).
820 51. S. M. Ghazi-Nouri, A. Assi, G. A. Limb, R. A. Scott, K. von Bussmann, I.
821 Humphrey, P. J. Luthert, D. G. Charteris, Laser photocoagulation alters the pattern of
822 staining for neurotrophin-4, GFAP, and CD68 in human retina. *Br J Ophthalmol* 87, 488-
823 492 (2003).
824 52. M. Simsek, S. Ozates, B. Gulpamuk, B. Buyukeren, M. Y. Teke, Dedifferentiation
825 of retinal pigment epithelium in a patient with chronic retinal detachment. *Ophthalmic*
826 *Surg Lasers Imaging Retina* 49, 716-720 (2018).
827 53. N. Josifovska, X. Lumi, M. Szatmari-Toth, E. Kristof, G. Russell, R. Nagymihaly, N.
828 Anisimova, B. Malyugin, M. Kolko, D. Ivastinovic, G. Petrovski, Clinical and molecular
829 markers in retinal detachment-From hyperreflective points to stem cells and
830 inflammation. *PLoS One* 14, e0217548 (2019).

831 54. J. P. Sarks, S. H. Sarks, M. C. Killingsworth, Evolution of geographic atrophy of the
832 retinal pigment epithelium. *Eye* 2, 552-577 (1988).
833 55. K. Gocho, V. Sarda, S. Falah, J. A. Sahel, M. Benchaboune, M. Ullern, M. Paques,
834 Adaptive optics imaging of geographic atrophy. *Invest Ophthalmol Vis Sci* 54, 3673-3680
835 (2013).
836 56. P. L. Penfold, M. C. Killingsworth, S. H. Sarks, Senile macular degeneration: the
837 involvement of immunocompetent cells. *Graefes Arch Clin Exp Ophthalmol* 223, 69-76.
838 (1985).
839 57. F. Sennlaub, C. Auvynet, B. Calippe, S. Lavalette, L. Poupel, S. J. Hu, E.
840 Dominguez, S. Camelo, O. Levy, E. Guyon, N. Saederup, I. F. Charo, N. V. Rooijen, E.
841 Nandrot, J. L. Bourges, F. Behar-Cohen, J. A. Sahel, X. Guillonneau, W. Raoul, C.
842 Combadiere, CCR2(+) monocytes infiltrate atrophic lesions in age-related macular
843 disease and mediate photoreceptor degeneration in experimental subretinal
844 inflammation in Cx3cr1 deficient mice. *EMBO Mol Med* 5, 1775-1793 (2013).
845 58. S. L. Schlereth, S. Kremers, F. Schrodl, C. Cursiefen, L. M. Heindl,
846 Characterization of antigen-presenting macrophages and dendritic cells in the healthy
847 human sclera. *Invest Ophthalmol Vis Sci* 57, 4878-4885 (2016).
848 59. M. F. Shirazi, E. Brunner, M. Laslandes, A. Pollreisz, C. K. Hitzenberger, M.
849 Pircher, Visualizing human photoreceptor and retinal pigment epithelium cell mosaics in
850 a single volume scan over an extended field of view with adaptive optics optical
851 coherence tomography. *Biomed. Opt. Express* 11, 4520-4535 (2020).
852 60. B. Lee, S. Chen, E. M. Moult, Y. Yu, A. Y. Alibhai, N. Mehta, C. R. Baumal, N. K.
853 Waheed, J. G. Fujimoto, High-speed, ultrahigh-resolution spectral-domain OCT with
854 extended imaging range using reference arm length matching. *Translational Vision*
855 *Science & Technology* 9, 12-12 (2020).
856 61. Z. Wu, C. D. Luu, L. A. B. Hodgson, E. Caruso, N. Tindill, K. Z. Aung, M. B.
857 McGuinness, G. Makeyeva, F. K. Chen, U. Chakravarthy, J. J. Arnold, W. J. Heriot, S. R.
858 Durkin, R. H. Guymer, Prospective longitudinal evaluation of nascent geographic atrophy
859 in age-related macular degeneration. *Ophthalmol Retina*, (2019).
860 62. R. Dolz-Marco, K. M. Litts, A. C. S. Tan, K. B. Freund, C. A. Curcio, The evolution
861 of outer retinal tubulation, a neurodegeneration and gliosis prominent in macular
862 diseases. *Ophthalmology* 124, 1353-1367 (2017).
863 63. M. M. Edwards, D. S. McLeod, I. A. Bhutto, R. Grebe, M. Duffy, G. A. Lutty,
864 Subretinal glial membranes in eyes with geographic atrophy. *Invest Ophthalmol Vis Sci*
865 58, 1352-1367 (2017).
866 64. L. Chen, J. D. Messinger, D. Ferrara, K. B. Freund, C. A. Curcio, Stages of drusen-
867 associated atrophy in age-related macular degeneration visible via histologically
868 validated fundus autofluorescence. *Ophthalmology Retina* 11/30/20 online, (2020).
869 65. B. Lujan, A. Roorda, R. W. Knighton, J. Carroll, Revealing Henle's fiber layer using
870 spectral domain optical coherence tomography. *Invest Ophthalmol Vis Sci* 52, 1486–
871 1492 (2011).
872 66. P. F. Stetson, Z. Yehoshua, C. A. Garcia Filho, R. Portella Nunes, G. Gregori, P. J.
873 Rosenfeld, OCT minimum intensity as a predictor of geographic atrophy enlargement.
874 *Invest Ophthalmol Vis Sci* 55, 792-800 (2014).
875 67. A. C. Tan, M. Pilgrim, S. Fearn, S. Bertazzo, E. Tsolaki, A. Morrell, M. Li, J. D.
876 Messinger, R. Dolz-Marco, M. G. Nittala, J. Lei, S. R. Sadda, I. Lengyel, K. B. Freund, C.
877 A. Curcio, Calcified nodules in retinal drusen are associated with disease progression
878 with age-related macular degeneration. *Sci Transl Med* 10, 466-477 (2018).

879 68. D. Pauleikhoff, C. A. Harper, J. Marshall, A. C. Bird, Aging changes in Bruch's
880 membrane: a histochemical and morphological study. *Ophthalmology* 97, 171-178
881 (1990).
882 69. C. A. Curcio, C. L. Millican, T. Bailey, H. S. Kruth, Accumulation of cholesterol with
883 age in human Bruch's membrane. *Invest. Ophthalmol. Vis. Sci.* 42, 265-274 (2001).
884 70. R. F. Mullins, M. N. Johnson, E. A. Faidley, J. M. Skeie, J. Huang, Choriocapillaris
885 vascular dropout related to density of drusen in human eyes with early age-related
886 macular degeneration. *Investigative ophthalmology & visual science* 52, 1606-1612
887 (2011).
888 71. L. Chen, J. D. Messinger, K. R. Sloan, T. A. Swain, Y. Sugiura, L. A. Yannuzzi, C.
889 A. Curcio, K. B. Freund, Non-exudative neovascularization supporting outer retina in
890 age-related macular degeneration, a clinicopathologic correlation. *Ophthalmology* 127,
891 931-947 (2020).
892 72. K. G. Chen, J. A. Alvarez, M. Yazdanie, C. Papudesu, W. T. Wong, H. Wiley, E. Y.
893 Chew, F. L. Ferris, 3rd, C. A. Cukras, Longitudinal study of dark adaptation as a
894 functional outcome measure for age-related macular degeneration. *Ophthalmology* 126,
895 856-865 (2019).
896 73. T. M. Redmond, S. Yu, E. Lee, D. Bok, D. Hamasaki, N. Chen, P. Goletz, J.-X. Ma,
897 R. K. Crouch, K. Pfeifer, *Rpe65* is necessary for production of 11-*cis*-vitamin A in the
898 retinal visual cycle. *Nature Genetics* 20, 344-351 (1998).
899 74. C. L. Nordgaard, K. M. Berg, R. J. Kapphahn, C. Reilly, X. Feng, T. W. Olsen, D. A.
900 Ferrington, Proteomics of the retinal pigment epithelium reveals altered protein
901 expression at progressive stages of age-related macular degeneration. *Invest*
902 *Ophthalmol Vis Sci* 47, 815-822 (2006).
903 75. C. Guidry, N. E. Medeiros, C. A. Curcio, Phenotypic variation of retinal pigment
904 epithelium in age-related macular degeneration. *Invest Ophthalmol Vis Sci* 43, 267-273.
905 (2002).
906 76. S. Ghosh, P. Shang, H. Terasaki, N. Stepicheva, S. Hose, M. Yazdankhah, J.
907 Weiss, T. Sakamoto, I. A. Bhutto, S. Xia, J. S. Zigler, Jr., R. Kannan, J. Qian, J. T.
908 Handa, D. Sinha, A role for betaA3/A1-crystallin in Type 2 EMT of RPE cells occurring in
909 dry age-related macular degeneration. *Invest Ophthalmol Vis Sci* 59, AMD104-AMD113
910 (2018).
911 77. M. Zhou, J. S. Geathers, S. L. Grillo, S. R. Weber, W. Wang, Y. Zhao, J. M.
912 Sundstrom, Role of epithelial-mesenchymal transition in retinal pigment epithelium
913 dysfunction. *Front Cell Dev Biol* 8, 501 (2020).
914 78. I. A. Bhutto, D. S. McLeod, C. Merges, T. Hasegawa, G. A. Lutty, Localisation of
915 SDF-1 and its receptor CXCR4 in retina and choroid of aged human eyes and in eyes
916 with age related macular degeneration. *Br J Ophthalmol* 90, 906-910 (2006).
917 79. H. Kaneko, S. Dridi, V. Tarallo, B. D. Gelfand, B. J. Fowler, W. G. Cho, M. E.
918 Kleinman, S. L. Ponicsan, W. W. Hauswirth, V. A. Chiodo, K. Kariko, J. W. Yoo, D. K.
919 Lee, M. Hadziahmetovic, Y. Song, S. Misra, G. Chaudhuri, F. W. Buaas, R. E. Braun, D.
920 R. Hinton, Q. Zhang, H. E. Grossniklaus, J. M. Provis, M. C. Madigan, A. H. Milam, N. L.
921 Justice, R. J. Albuquerque, A. D. Blandford, S. Bogdanovich, Y. Hirano, J. Witta, E.
922 Fuchs, D. R. Littman, B. K. Ambati, C. M. Rudin, M. M. Chong, P. Provost, J. F. Kugel, J.
923 A. Goodrich, J. L. Dunaief, J. Z. Baffi, J. Ambati, DICER1 deficit induces *Alu* RNA toxicity
924 in age-related macular degeneration. *Nature* 471, 325-330 (2011).

925 80. M. R. Terluk, R. J. Kapphahn, L. M. Soukup, H. Gong, C. Gallardo, S. R.
926 Montezuma, D. A. Ferrington, Investigating mitochondria as a target for treating age-
927 related macular degeneration. *J Neurosci* 35, 7304-7311 (2015).
928 81. S. Notomi, K. Ishihara, N. E. Efstathiou, J. J. Lee, T. Hisatomi, T. Tachibana, E. K.
929 Konstantinou, T. Ueta, Y. Murakami, D. E. Maidana, Y. Ikeda, S. Kume, H. Terasaki, S.
930 Sonoda, J. Blanz, L. Young, T. Sakamoto, K. H. Sonoda, P. Saftig, T. Ishibashi, J. W.
931 Miller, G. Kroemer, D. G. Vavvas, Genetic LAMP2 deficiency accelerates the age-
932 associated formation of basal laminar deposits in the retina. *Proc Natl Acad Sci U S A*
933 116, 23724-23734 (2019).
934 82. J. A. Gambril, K. R. Sloan, T. A. Swain, C. Huisingh, A. V. Zarubina, J. D.
935 Messinger, T. Ach, C. A. Curcio, Quantifying retinal pigment epithelium dysmorphia and
936 loss of histologic autofluorescence in age-related macular degeneration. *Invest*
937 *Ophthalmol Vis Sci* 60, 2481-2493 (2019).
938 83. G. Staurenghi, S. Sadda, U. Chakravarthy, R. F. Spaide, Proposed lexicon for
939 anatomic landmarks in normal posterior segment spectral-domain optical coherence
940 tomography: The IN*OCT Consensus. *Ophthalmology* 121, 1572-1578 (2014).
941 84. A. A. Sura, L. Chen, J. D. Messinger, T. A. Swain, G. McGwin Jr, K. B. Freund, C.
942 A. Curcio, Measuring the contributions of basal laminar deposit and Bruch's membrane
943 in age-related macular degeneration. *Invest Ophthalmol Vis Sci* 61, 19 (2020).
944 85. A. C. S. Tan, K. B. Freund, C. Balaratnasingam, D. Simhaee, L. A. Yannuzzi,
945 Imaging of pigment epithelial detachments with optical coherence tomography
946 angiography. *Retina* 38, 1759-1769 (2018).
947 86. F. A. Jakobiec, P. C. Barrantes, Y. Yonekawa, E. M. Lad, A. D. Proia, Subretinal
948 mononuclear cells in Coats' disease studied with RPE65 and CD163: evidence for
949 histiocytoid pigment epithelial cells. *American Journal of Ophthalmology* 222, 388-396
950 (2020).
951 87. A. Bringmann, S. Syrbe, K. Gorner, J. Kacza, M. Francke, P. Wiedemann, A.
952 Reichenbach, The primate fovea: Structure, function and development. *Prog Retin Eye*
953 *Res* 66, 49-84 (2018).
954 88. J. Monés, M. Biarnes, F. Trindade, Hyporeflective wedge-shaped band in
955 geographic atrophy secondary to age-related macular degeneration: an underreported
956 finding. *Ophthalmology* 119, 1412-1419 (2012).
957 89. C. Cukras, E. Agron, M. L. Klein, F. L. Ferris, 3rd, E. Y. Chew, G. Gensler, W. T.
958 Wong, Natural history of drusenoid pigment epithelial detachment in age-related macular
959 degeneration: Age-Related Eye Disease Study Report No. 28. *Ophthalmology* 117, 489-
960 499 (2010).
961 90. J. J. Arnold, J. P. Sarks, M. C. Killingsworth, E. K. Kettle, S. H. Sarks, Adult
962 vitelliform macular degeneration: a clinicopathological study. *Eye* 17, 717-726. (2003).
963